Intestinal barrier dysfunction orchestrates the onset of inflammatory host–microbiome cross-talk in a human gut inflammation-on-a-chip

Woojung Shin[a] and Hyun Jung Kim[a,b,1]

[a]Department of Biomedical Engineering, The University of Texas at Austin, Austin, TX 78712; and [b]Department of Medical Engineering, Yonsei University College of Medicine, 03722 Seoul, Republic of Korea

Edited by Ralph R. Isberg, Howard Hughes Medical Institute and Tufts University School of Medicine, Boston, MA, and approved October 3, 2018 (received for review June 23, 2018)

The initiation of intestinal inflammation involves complex intercellular cross-talk of inflammatory cells, including the epithelial and immune cells, and the gut microbiome. This multicellular complexity has hampered the identification of the trigger that orchestrates the onset of intestinal inflammation. To identify the initiator of inflammatory host–microbiome cross-talk, we leveraged a pathomimetic "gut inflammation-on-a-chip" undergoing physiological flow and motions that recapitulates the pathophysiology of dextran sodium sulfate (DSS)-induced inflammation in murine models. DSS treatment significantly impaired, without cytotoxic damage, epithelial barrier integrity, villous microarchitecture, and mucus production, which were rapidly recovered after cessation of DSS treatment. We found that the direct contact of DSS-sensitized epithelium and immune cells elevates oxidative stress, in which the luminal microbial stimulation elicited the production of inflammatory cytokines and immune cell recruitment. In contrast, an intact intestinal barrier successfully suppressed oxidative stress and inflammatory cytokine production against the physiological level of lipopolysaccharide or nonpathogenic *Escherichia coli* in the presence of immune elements. Probiotic treatment effectively reduced the oxidative stress, but it failed to ameliorate the epithelial barrier dysfunction and proinflammatory response when the probiotic administration happened after the DSS-induced barrier disruption. Maintenance of epithelial barrier function was necessary and sufficient to control the physiological oxidative stress and proinflammatory cascades, suggesting that "good fences make good neighbors." Thus, the modular gut inflammation-on-a-chip identifies the mechanistic contribution of barrier dysfunction mediated by intercellular host–microbiome cross-talk to the onset of intestinal inflammation.

gut inflammation-on-a-chip | microbiome | barrier function | inflammation | disease model

Human intestinal inflammation involves complex pathophysiological processes including mucosal injury (1), impaired barrier function (2), recruitment and infiltration of immune cells (3), and subsequent inflammatory responses including secretion of inflammatory cytokines (4). Compromised biomechanical dynamics in the gut is also closely associated with the pathophysiology of gut inflammation (5). Animal models (6, 7) and human clinical studies (8) for intestinal inflammation have revealed that the aberrant intercellular interaction between epithelium, gut microbiome, and immune components is the major contributing factor that causes inflammatory pathogenesis in the gut. Indeed, the pathogenic manifestation in inflammatory bowel disease (IBD) has been characterized as a "leaky gut" (9), dysbiosed gut microbiome (10), and hyperactivated immunity (8, 11).

Thus, identification of the key modulator that orchestrates the onset of inflammatory responses in the gut is of great importance because this identification would support the development of clinical and therapeutic options that target the prime initiator of the whole inflammatory cascades. Identification of the inflammatory trigger is also decisive for developing more accurate, target-specific antiinflammatory agents (12). However, it has been challenging to identify the initiating factor of gut inflammation because it is not possible to independently manipulate these complex parameters in current inflammation models. For instance, animal surrogates and in vitro cell culture models have been suggested to study intestinal inflammatory mechanism (6) or validate the efficacy of antiinflammatory drugs (13, 14). Although multiple animal inflammation models that rely on chemical (15), genetic (16, 17), or immunological treatment (18) have been developed (6), it has not been possible to independently uncouple each contributing factor in a spatiotemporal manner. In vitro cell culture models are simple and robust for studying intestinal inflammation. However, human intestinal cell lines often undergo poor tissue-specific histogenesis, differentiation, and physiological functions (19–21). Furthermore, the static nature of in vitro cultures does not support the longitudinal investigation of host–microbiome interactions because these cultures are subject to bacterial overgrowth, depletion of nutrients, and accumulation of metabolic wastes (20, 22, 23). Thus, development of a modular model of human gut inflammation that can add, remove, and exchange inflammatory factors at various complexities is important to emulate intercellular host–microbiome cross-talk during inflammation.

Significance

Identification of the trigger of human intestinal inflammation can be a compelling clinical strategy for developing effective and target-specific antiinflammatory therapeutics. The pathomimetic "gut inflammation-on-a-chip" inspired by dextran sodium sulfate (DSS)-induced colitis models in mice enabled the independent uncoupling of complex inflammatory cross-talks and the combinatorial recoupling of individual contributing factors one at a time to identify the initiator of inflammatory responses. Our discovery suggests that an intact epithelial barrier is necessary to maintain the "homeostatic tolerance" in response to physiological host–gut microbiome cross-talks. We also expound an insight of probiotic therapy that the undamaged epithelial barrier is a prerequisite for eliciting the probiotic efficacy. Finally, the gut inflammation-on-a-chip verifies how microphysiological systems can be successfully implemented to dissect the mechanisms of gastrointestinal diseases.

Author contributions: W.S. and H.J.K. designed research, performed research, analyzed data, and wrote the paper.

The authors declare no conflict of interest.

This article is a PNAS Direct Submission.

[1]To whom correspondence should be addressed. Email: hyunjung.kim@utexas.edu.

This article contains supporting information online at www.pnas.org/lookup/suppl/doi:10.1073/pnas.1810819115/-/DCSupplemental.

Published online October 22, 2018.

We previously developed a human gut-on-a-chip to demonstrate the mechanically dynamic microenvironment of the living human intestine (20) that undergoes epithelial villus growth (21), lineage-dependent cytodifferentiation (21), enhanced mucus production and barrier function (20, 21), long-term host–microbiome coculture (20, 24), pathogenic infection (24), inflammatory immune–microbiome interaction (24), and microbial overgrowth syndrome under the cessation of peristalsis-like deformations (24). In this present study, we utilized a human "gut inflammation-on-a-chip" to investigate the intercellular host–microbiome cross-talk during chemically induced inflammation and identify the seminal initiator of the overall inflammatory cascade. We accurately manipulated the integrity of the epithelial barrier by adding or removing dextran sodium sulfate (DSS), a chemical reagent that causes colitis in animal models (25, 26). By controlling the barrier function, we established and analyzed an inflammatory milieu that involves microenvironmental cross-talk. This milieu enabled us to seek out a critical component that initiates and orchestrates the aberrant intercellular interactions and inflammatory responses. Finally, as a proof-of-principle, we harnessed this gut inflammation-on-a-chip to elucidate the consequence of probiotic treatment under barrier dysfunction, which may have clinical and pharmaceutical potentials to determine the best practices for probiotic or microbiome-based therapeutics.

Results

Decoupling the Complex Intercellular Cross-Talk On-Chip. To investigate the spatiotemporal contribution of intestinal microenvironmental factors to the onset of inflammation, we leveraged a gut-on-a-chip microfluidic device (20, 21) made of elastic silicone polymer (polydimethylsiloxane, PDMS). This microdevice contains two compartments separated by a porous, flexible, extracellular matrix (ECM)-coated PDMS membrane, in which the upper–lower compartments represent the lumen–capillary interface in the human intestine. In this 3D structure, we set out minimal but necessary components that are directly associated with intestinal inflammatory cross-talk. The lumen microchannel contains human intestinal Caco-2 villi (20, 21), in which DSS was used as a "negative regulator" of the epithelial barrier function. By adding or removing the intestinal microenvironmental factors in the lumen (e.g., nonpathogenic *Escherichia coli*, probiotic VSL#3, and lipopolysaccharide (LPS) endotoxin) and the capillary layers (e.g., peripheral blood mononuclear cells, PBMCs) in a spatiotemporal manner, we manipulated the induction of complex immune responses in vitro (Fig. 1*A*).

DSS-Induced Intestinal Barrier Dysfunction. To recreate the DSS-induced intestinal inflammation that has been demonstrated in mouse models (25, 26), we introduced DSS to the luminal compartment of the villi, mimicking the gavage of DSS in a mouse model. We determined to use 2% (wt/vol) of DSS (40 kDa) in this study, based on the most significant increase ($P < 0.0001$) of the transport of a paracellular marker (FITC-dextran, 20 kDa; *SI Appendix*, Fig. S1). When DSS was introduced to the lumen side of the villi experienced with continuous flow (50 μL/h, corresponding shear stress at 0.02 dyne/cm^2)

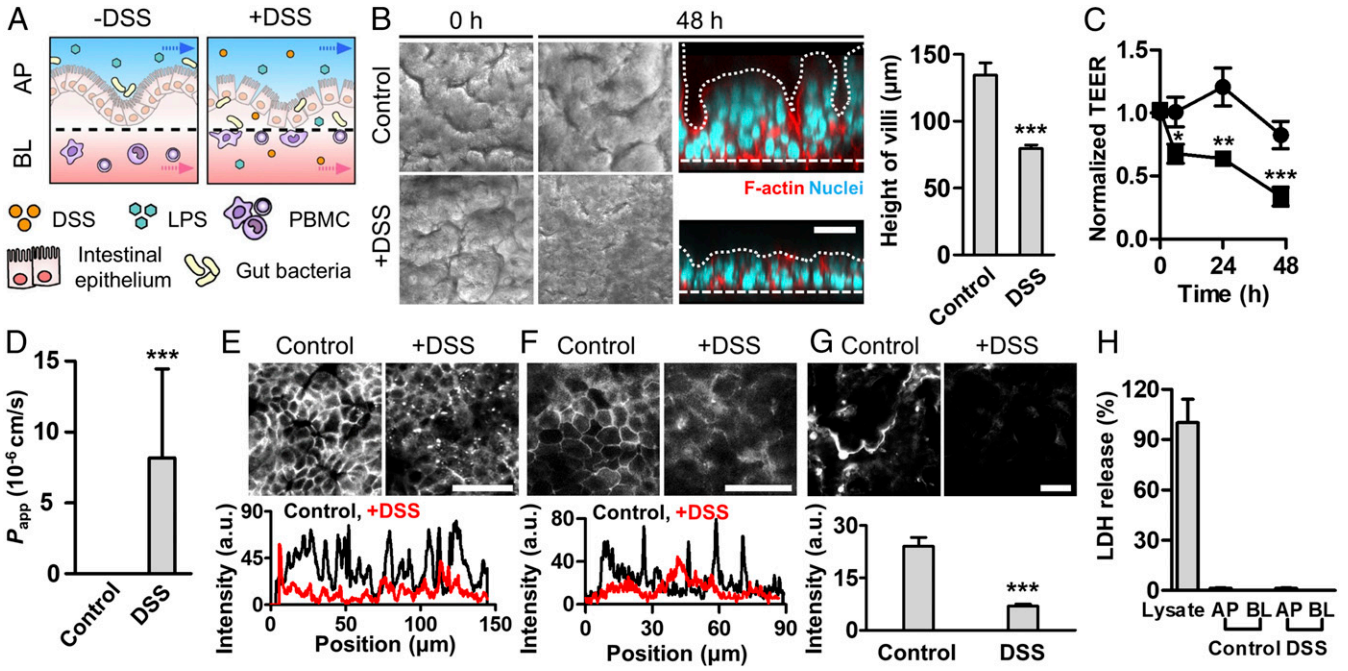

Fig. 1. Administration of DSS specifically induces epithelial barrier dysfunction in a gut inflammation-on-a-chip. (*A*) An experimental design that describes the microenvironment of the human intestine undergoing DSS-mediated epithelial barrier dysfunction and subsequent transmigration of gut bacteria and immune cells (+DSS) compared with the normal healthy condition (−DSS). AP, apical; BL, basolateral. (*B*) Morphology of the villus epithelium visualized by the differential interference contrast (DIC) (gray, top views) and immunofluorescence (IF) microscopy (colored, side views) at 0 and 48 h after DSS treatment (2%, wt/vol). A white dashed line indicates the location of a porous basement membrane. A white dotted line indicates the contour of villous microarchitecture. The height of villi was measured by analyzing IF micrographs of the vertical cross-cut view ($n = 7$). (*C*) Intestinal barrier function of the control intestinal villi (circle; $n = 10$) compared with the villi challenged to 2% (wt/vol) DSS (square; $n = 10$) quantitated by TEER. (*D*) Apparent permeability of a paracellular marker (FITC-dextran; 20 kDa) through the villous epithelial layer in the absence (Control) or the presence of DSS (DSS) ($n = 3$). Permeability values of the Control was below the detection range. Localization of E-cadherin adherens junction (*E*) and ZO-1 tight junction proteins (*F*) (*Upper*) and the line scan of corresponding IF images (*Lower*) in the absence (Control) or the presence of DSS treatment (+DSS) for 48 h. (*G*) Visualization of the mucus layer via IF staining with Alexa Fluor 633-conjugated WGA at 48 h after DSS treatment (*Upper*) and its quantification (*Lower*) ($n = 8$). (*H*) Epithelial cytotoxicity in response to the DSS treatment quantitated by an lactic acid dehydrogenase (LDH) assay. The culture medium collected from the AP and BL microchannels in the gut inflammation-on-a-chip challenged to DSS for 48 h did not show any LDH release. Cell lysate of Caco-2 cells grown on a chip was used as a positive control ($n = 10$). (Scale bars, 50 μm.) *$P < 0.05$, **$P < 0.001$, ***$P < 0.0001$.

and peristalsis-like cyclic rhythmical deformations (10% in cell strain, 0.15 Hz in frequency) (20, 21, 27), villus epithelium progressively lost its microstructure as a function of time (Fig. 1*B* and *SI Appendix*, Fig. S2). DSS treatment caused substantial atrophic villous blunting (h = 76.6 ± 2.9 μm) compared with the control (h = 134 ± 9.1 μm; Fig. 1*B*, *Right*). DSS treatment also induced a significant decrease of barrier integrity as measured by transepithelial electrical resistance (TEER) (Fig. 1*C*), which resulted in a drastic increase of apparent permeability (P_{app}; 8.17 ± 6.27 × 10^{-6} cm/s) compared with the control (Fig. 1*D*). The presence of DSS led to the compromised expression of E-cadherin (Fig. 1*E*) and ZO-1 (Fig. 1*F*) visualized by the immunofluorescence (IF) staining on the villus epithelium, whereas the absence of DSS allowed a uniform and stable distribution of junctional protein expression across the villus structure. The DSS-challenged epithelium showed the significant reduction of intestinal mucus production quantitated by wheat germ agglutinin (WGA) (28) (Fig. 1*G*) and mucin 2 (MUC2)-positive epithelial cells (*SI Appendix*, Fig. S3), suggesting that the DSS-induced barrier dysfunction may be attributed to the disruption of a mucus layer. However, the addition of DSS neither directly induced epithelial cytotoxicity (Fig. 1*H* and *SI Appendix*, Figs. S4*A* and S7*A*) nor compromised epithelial viability (*SI Appendix*, Figs. S4*B*, S5, S6, and S7*B*), suggesting that the DSS treatment specifically and robustly disrupts the intestinal epithelial barrier without causing any cytotoxic injuries to the epithelium. Interestingly, the cessation of DSS treatment rapidly restored the TEER value to the level of the DSS-untreated control (Fig. 2*A*), indicating that the intestinal barrier integrity is controllable and responsive to DSS treatment. While DSS treatment caused disrupted epithelial structure (Fig. 2*B*), decreased mucus production (Fig. 2*C*), and compromised expression and localization of the tight junction ZO-1 protein (Fig. 2*D*), the removal of DSS resulted in the restoration of all these pathophysiological outcomes (Fig. 2 *B*–*D*, DSS ceased). Based on this controllable DSS-directed barrier dysfunction, we specifically manipulated the barrier integrity to identify the onset trigger of inflammation during host–microbiome cross-talk.

Oxidative Stress During Immune–Epithelial Cross-Talk. Oxidative stress mediated by the generation of reactive oxygen species (ROS) is an early-stage trigger of the intestinal inflammation (29). Using a fluorogenic probe (30) that detects epithelial cytoplasmic free radicals, we investigated how the epithelial barrier dysfunction orchestrates oxidative stress during immune–epithelial cross-talk by combinatorially introducing luminal (DSS, LPS, and non-pathogenic *E. coli*) and capillary components (PBMC) to the apical and basolateral microchannels, respectively. When the epithelial barrier was intact without DSS challenges, the villus epithelium did not undergo any ROS-associated oxidative stress despite the costimulation of PBMC and LPS or *E. coli* cells (Fig. 3*A*, *Upper*). However, the intercellular cross-talk between the DSS-treated epithelium and PBMC significantly increased the cytoplasmic ROS level (Fig. 3*A*, +PBMC and +DSS), whereas DSS alone did not induce oxidative stress on both the epithelium (Fig. 3*A*, Control and +DSS) and the PBMC (*SI Appendix*, Fig. S10*A*, DSS). It is notable that the level of free radicals generated during the immune–epithelial cross-talk was almost identical to the level of the groups that contain bacterial LPS endotoxins at the physiological level (10 ng/mL) (31) or *E. coli* cells with a multiplicity of infections (MOIs) at 0.25. Up-regulation of the nuclear factor erythroid 2-related factor 2 (Nrf2) in PBMC supported the elevated oxidative stress in the mucosal microenvironment (Fig. 3*B*). We found that the addition of PBMC triggers ROS generation through the direct contact to DSS-sensitized "leaky" epithelium in both static Transwell and microfluidic cultures. When the DSS-treated epithelium grown on the Transwell inserts with different pore sizes (0.4 vs. 8.0 μm) was challenged to PBMC on

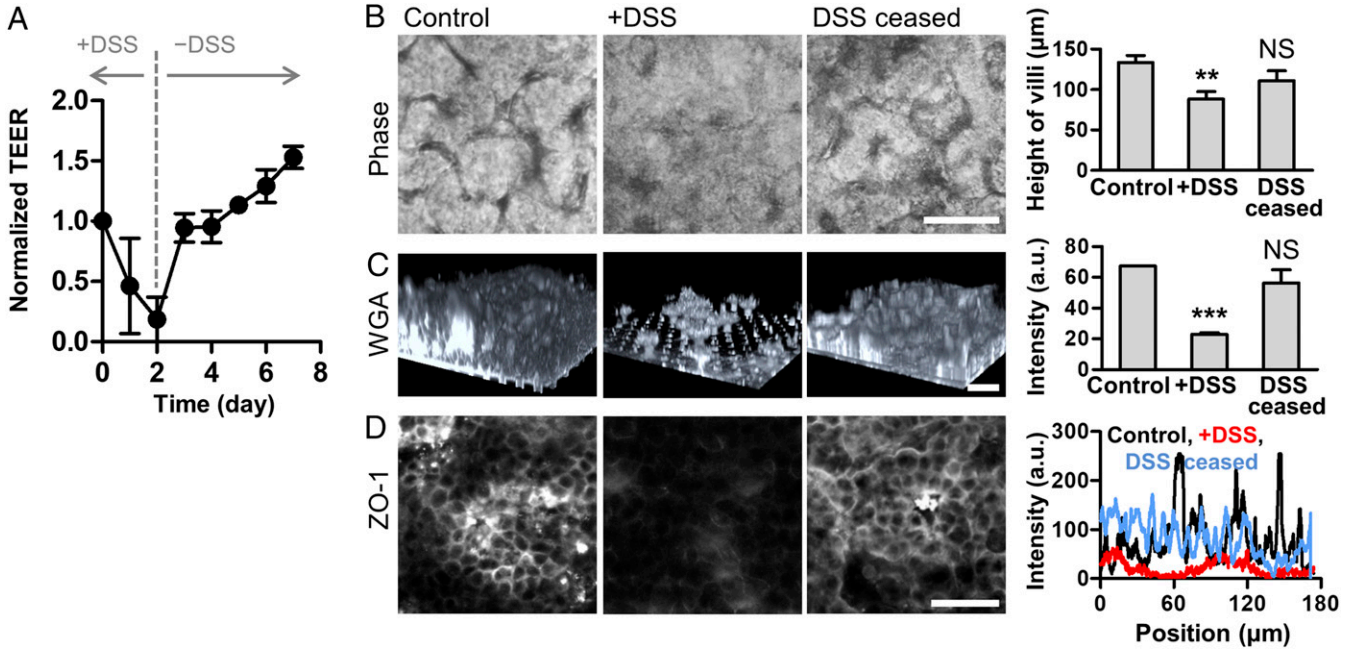

Fig. 2. Recovery of barrier dysfunction after the cessation of DSS treatment. (*A*) Restoration of the barrier function in response to the DSS treatment (+DSS) and its cessation (−DSS) measured by TEER ($n = 2$). Intestinal villi were challenged to DSS (2%, wt/vol) for 2 d and then further cultured without DSS treatment for an additional 5 d. (*B*) Phase contrast images showing intestinal villous microstructure before (Control) and after the DSS treatment for 48 h (+DSS). Microengineered villus structure was recovered when DSS was ceased for an additional 48 h (DSS ceased), and the quantification of the height of villi (*Right*, $n = 5$). (*C*) Visualization of the mucus production highlighted by the Alexa Fluor 633-conjugated WGA. A 3D reconstruction of Z-stacked images is shown. Quantification of the averaged intensity of each 3D reconstructed image was performed using ImageJ (*Right*, $n = 2$). (*D*) Localization of tight junction protein ZO-1 (*Left*) and a line scan snapshot in each experimental group (*Right*). (Scale bars, 50 μm.) NS, not significant. $^{**}P < 0.001$, $^{***}P < 0.0001$.

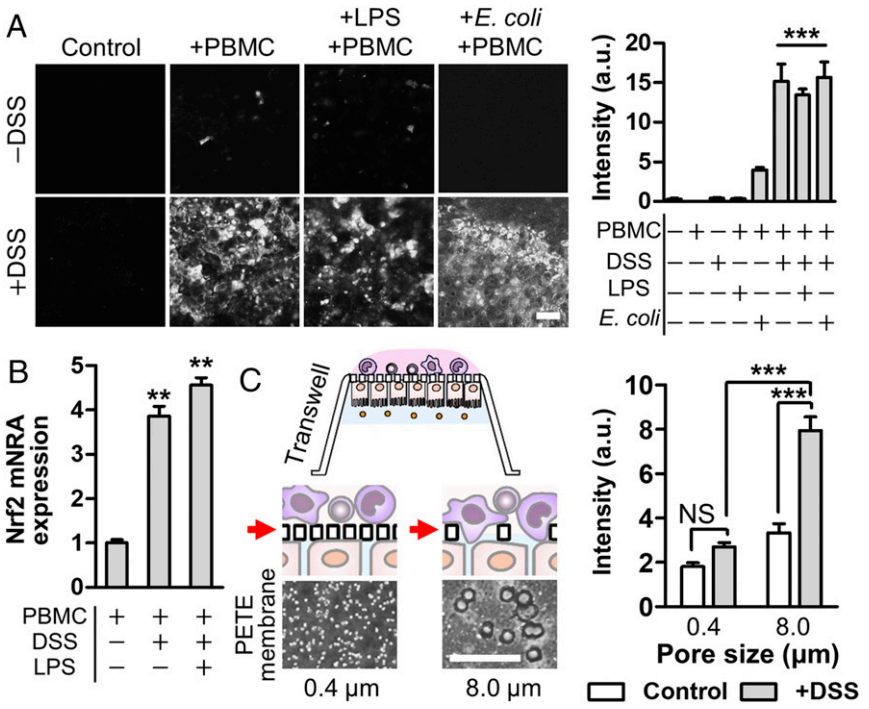

Fig. 3. Direct cross-talk of the barrier-compromised epithelium and immune components induces cytoplasmic oxidative stress. (*A*) Production of ROS visualized by the fluorescence probe (CellROX) that detects free radicals in the cytoplasm at 24 h after introduction of PBMCs. Images were analyzed to quantify the fluorescence intensity using ImageJ ($n = 10$). (*B*) Expression profile of Nrf2 gene in PBMC after the epithelial–immune cross-talk was performed in the presence of DSS alone or DSS and LPS together in the gut inflammation-on-a-chip. Cells were harvested at 24 h after PBMCs were introduced into the basolateral microchannel ($n = 2$). (*C*) Direct contact effect between PBMC and DSS-sensitized epithelium was assessed in the Transwell insert with either 0.4- or 8.0-μm pores, respectively. Phase contrast images of a polyester track-etched (PETE) membrane in each Transwell insert were provided below the schematic. White holes show the pores in each membrane. Quantification of the oxidative stress of Caco-2 cells grown on each porous insert (0.4 vs. 8.0 μm) that underwent costimulation with DSS and PBMC (2×10^4 cells per insert) in the AP and BL compartments, respectively ($n = 89$). (Scale bars, 50 μm.) NS, not significant. $^{**}P < 0.001$, $^{***}P < 0.0001$.

the opposite side of a porous membrane (Fig. 3*C*, schematic), the epithelium on an 8.0-μm insert produced an approximately threefold increased ROS ($P < 0.0001$) compared with the epithelium on a 0.4-μm insert (Fig. 3*C*). Direct introduction of PBMC into the apical side of the DSS-challenged epithelium significantly ($P < 0.0001$) increased the epithelial ROS (~4.5-fold) compared with the addition of PBMC in the lower microchannel (*SI Appendix*, Fig. S8). We also confirmed that the presence of detached DSS-sensitized epithelium in the conditioned medium significantly induced ROS production in PBMC (*SI Appendix*, Fig. S10*A*, +DSS, AP and +DSS, pellet, AP), whereas the cell-free conditioned medium did not show any significant level of ROS (*SI Appendix*, Fig. S10 *A* and *B*). On the contrary, PBMC failed to induce oxidative stress in the intact "healthy" epithelium regardless of its direct contact with the epithelium in both the chip (Fig. 3*A*, +PBMC and −DSS) and the Transwell (*SI Appendix*, Fig. S9). Taken together, these findings indicate that the cytoplasmic ROS generation requires intercellular cross-talk through direct contact between immune cells and the barrier-compromised epithelium.

Effect of Epithelial Barrier Dysfunction on Inflammatory Responses. Next, we quantitatively assessed the production of representative proinflammatory cytokines such as interleukin (IL)-1β, IL-6, and tumor necrosis factor (TNF)-α in response to the intestinal barrier dysfunction. When the villus epithelium was simultaneously challenged to both DSS and PBMC without any luminal components (e.g., bacterial cells or LPS), epithelium did not produce any detectable amount of IL-1β, IL-6, or TNF-α (Fig. 4*A*, +DSS) regardless of the strong ROS generation (Fig. 3*A*) or the long-term treatment of DSS (*SI Appendix*, Fig. S11). However, when the LPS at the physiological level (10 ng/mL) or *E. coli* cells (MOI, 0.25) were added in the lumen microchannel, the DSS-sensitized, PBMC-challenged epithelium induced drastic production of proinflammatory cytokines into the basolateral compartment (Fig. 4*A*, +DSS, +LPS and +DSS, +*E. coli*), morphological damages in villi (Fig. 4*B*, *Left*), recruitment and infiltration of PBMC at the basolateral area of villi (Fig. 4 *B*, *Right Insets* and Fig. 4*C*), decreased villous height (Fig. 4*D*), and impaired intestinal barrier function (Fig. 4*E*). In contrast, the physically intact epithelial barrier successfully prevented all of those pathological responses despite the costimulation of luminal and immune components in a spatiotemporal manner (Fig. 4 and *SI Appendix*, Figs. S11 and S12). It is noted that the presence of PBMC was necessary to initiate ROS generation (Fig. 3*A*) and the production of proinflammatory cytokines (Fig. 4*A* and *SI Appendix*, Fig. S12), but all of these inflammatory responses were only manifested under the epithelial barrier impairment (Fig. 4).

Recapitulating Conditional Probiotic Efficacy Under Barrier Dysfunction. The compromised epithelial barrier not only initiated the inflammatory response but also substantially altered the therapeutic efficacy of probiotic treatment (32–34). To investigate how barrier dysfunction perturbs the therapeutic efficacy of probiotic treatment, we cocultured eight strains of probiotic gut bacteria (VSL#3) in the gut inflammation-on-a-chip in which the addition of VSL#3 cells was varied before ("pretreatment") or after ("posttreatment") the DSS-induced barrier disruption in the presence of PBMC. As we previously demonstrated (24), coculture with probiotic VSL#3 bacteria significantly increased ($P < 0.001$) the barrier integrity of an intact villus epithelium measured by TEER (Fig. 5*A*, filled

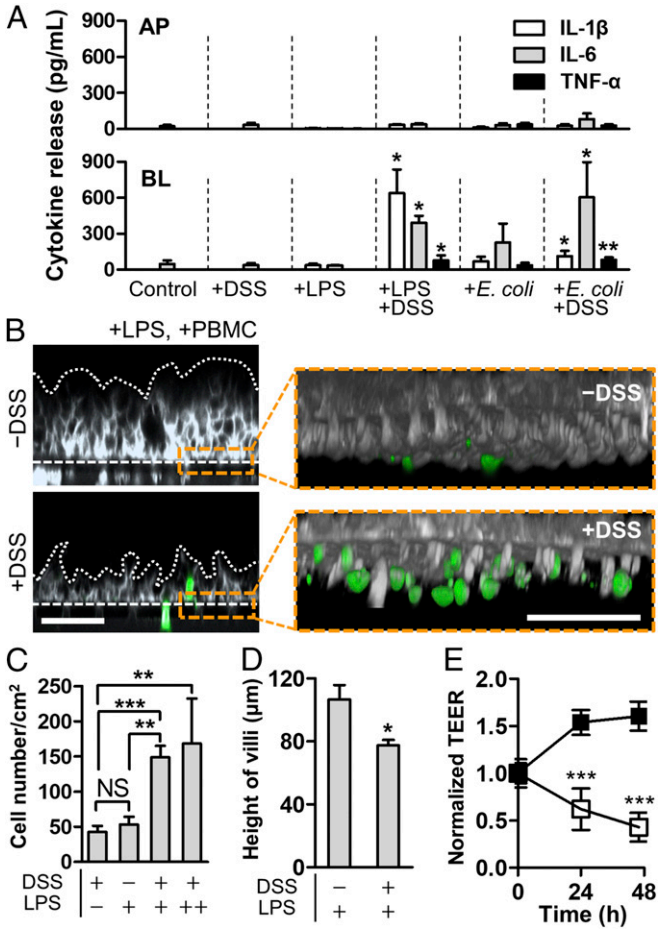

Fig. 4. Pathophysiological cross-talk between the barrier-impaired villus epithelium, gut microbiome or microbial LPS, and immune components exerts inflammatory responses. (*A*) Directional secretion of proinflammatory cytokines after costimulation of LPS (10 ng/mL) or *E. coli* cells (1×10^6 cfu/mL; MOI, 0.25) with PBMC (4×10^6 cells per milliliter) for 24 h in the presence or the absence of DSS treatment ($n = 4$). Statistical analysis was performed compared with the control group. (*B*) A cross-sectional view of the villus morphology (*Left*) and recruited immune cells (*Right Inset*) in response to apical DSS treatment. The villus epithelium was challenged to LPS (10 ng/mL) in the presence or the absence of DSS for 48 h, and then PBMC (4×10^6 cells per milliliter) was added to the BL side for 24 h. Villi were visualized by staining the plasma membrane of epithelial cells (gray) and PBMC (green). White dotted lines and dashed lines represent the contour of the villus epithelium and the location of porous membranes, respectively. (*C*) Quantification of the number of recruited PBMCs on the basolateral surface of the villus epithelium. In the LPS panel, "+" indicates the physiological concentration of LPS (10 ng/mL), whereas "++" represents the extremely high concentration of LPS (5 μg/mL) ($n = 8$). (*D*) Height of villi in response to the DSS treatment in the presence of LPS at the physiological level (10 ng/mL). (*E*) Effect of DSS-mediated barrier disruption of villus epithelium in response to LPS at physiological concentration (10 ng/mL). Intestinal barrier function displayed by the normalized TEER was declining in the presence of both DSS and LPS (open square), whereas the presence of LPS alone did not compromise any barrier function (filled square). All of the experimental groups include PBMCs (4×10^6 cells per milliliter). (Scale bars, 50 μm.) NS, not significant. $^*P < 0.05$, $^{**}P < 0.001$, $^{***}P < 0.0001$.

circle). It is noted that DSS did not hinder the growth of VSL#3 microbial cells (*SI Appendix*, Fig. S13 *A* and *E*). Thus, we anticipated that the probiotic treatment might contribute to ameliorating the barrier dysfunction. As expected, when intestinal villi were cocultured with the probiotic bacteria (initial MOI, 2.5) before the DSS treatment (pretreatment), the TEER value was maintained for 48 h with no significant difference from the control (Fig. 5*A*, filled square). However, when the villous epithelium was challenged to DSS before the administration of probiotic bacteria, the epithelium progressively lost the tight junction barrier regardless of the probiotic treatment (Fig. 5*A*, open square), impaired tight junction (Fig. 5*B* and *SI Appendix*, Fig. S14, ZO-1), and decreased mucus production (Fig. 5*B*, WGA). Interestingly, probiotic therapy substantially scavenged the cytoplasmic ROS (~52-fold reduction compared with the nonprobiotic control) without a significant difference between pre- and post-VSL#3 treatments (Fig. 5*C*). The epithelial barrier damage caused by the DSS treatment allowed the aberrant translocation of VSL#3 bacterial cells from the lumen to the capillary microchannel (Fig. 5*B*, Effluent culture), which significantly increased the directional secretion of proinflammatory cytokines (IL-1β, IL-6, and TNF-α) (Fig. 5*D*). When VSL#3 cells with the same MOI were directly introduced to PBMC in the absence of an epithelial layer, the amount of secreted inflammatory cytokines was ~85–200 times higher than those observed in the gut inflammation-on-a-chip (*SI Appendix*, Fig. S15), confirming that the intact intestinal barrier is critical for expecting the beneficial probiotic effect without aberrant immune responses.

Discussion

We report the successful in vitro identification of the initiating factor of human gut inflammation that involves complex intercellular host–microbiome cross-talks by leveraging a microengineered human gut inflammation-on-a-chip. The pathophysiological manifestation and intercellular responses during inflammation were recapitulated by accurately manipulating the epithelial barrier function inspired by DSS-induced colitis in murine models. We uncoupled each contributing factor, including gut epithelium, microbial cells and their cellular product (e.g., LPS), and immune components, and then combinatorially recoupled these factors one at a time to identify how each factor contributes to the initiation of inflammatory cross-talk and orchestrates the overall inflammatory milieu in a spatiotemporal manner. We identified that the control of epithelial barrier dysfunction is the key determinant for maintaining the homeostatic tolerance in the gut.

Experimental gastrointestinal (GI) surrogates and disease models have been suggested using microfluidic human organs-on-chips systems. These models have demonstrated the microarchitecture of human intestinal villi (20, 21, 35, 36), a lumen–capillary interface (24), peristalsis-like mechanical dynamics (20, 24), establishment of a host–microbiome ecosystem (20, 24, 37), gut inflammation and immune responses (24), small intestinal bacterial overgrowth (24), and radiation injury-induced cell damage (38). While these studies have focused on the demonstration of an in vivo relevant microstructure, physiological functions, and pathological outcomes at various exogenous stimulations as a proof-of-principle, our present study provides a mechanistic investigation to identify the initiator of the complex intercellular cross-talks that occur in the inflammatory intestinal microenvironment.

Since the intestinal inflammation involves a complicated cascade of intercellular cross-talks that switches on the immune-mediated ROS generation (39) and the activation of the intracellular nuclear factor (NF)–κB pathway (11), the development of a disease model that can modulate this pathophysiological complexity by uncoupling its individual components is crucial for dissecting the disease mechanisms. Although existing mouse inflammation models established by chemical (15), immunological (18), genetic (16, 17, 40), or spontaneous inductions (41, 42) are useful as in vivo experimental tools for showing pathological outcomes and systemic dysfunctions in inflammation, they are extremely limited to independently control and manipulate the key contributing factors during the intercellular interactions. In contrast, our gut inflammation-on-a-chip enables presenting the on-demand modularity, by which a snapshot of pathophysiological barrier dysfunction (e.g., leaky gut on the epithelium), immune-associated

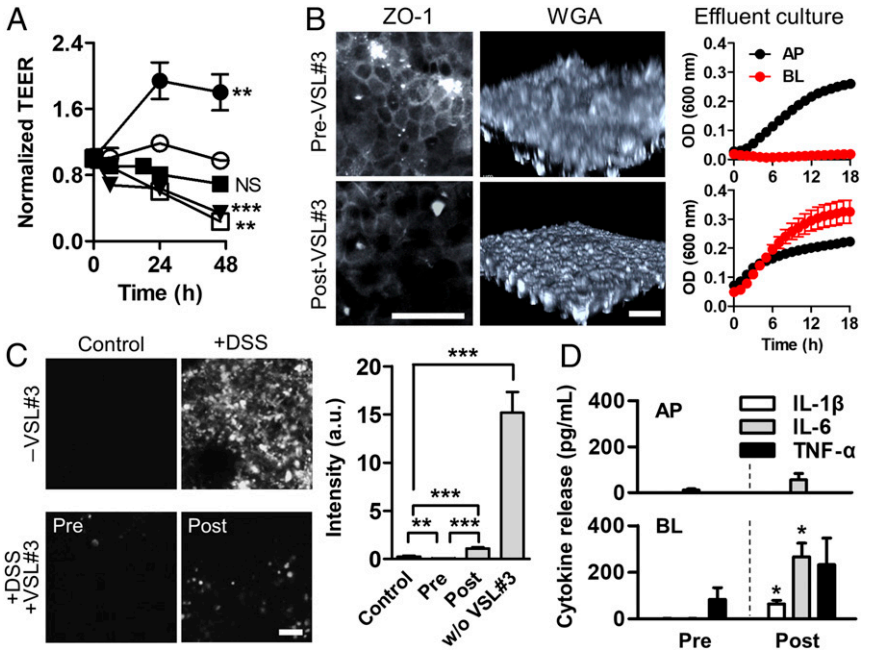

Fig. 5. Barrier dysfunction alters the probiotic efficacy. (*A*) Effect of the administration of probiotic VSL#3 and the DSS-mediated barrier dysfunction on the intestinal barrier function. VSL#3 (1×10^7 cfu/mL; MOI, 2.5) was treated at 0 h in +VSL#3 (filled circle). VSL#3 cells were inoculated to intestinal epithelium before (+DSS, Pre-VSL#3, filled square; preculture of VSL#3 for 24 h) or subsequent to (+DSS, Post-VSL#3, open square; postculture of VSL#3 for 24 h) the DSS treatment. Control (open circle); +DSS without VSL#3 (inverted triangle). (*B*) Visualization of the localized tight junction ZO-1 (ZO-1) and the mucus production (WGA), and the growth profile of VSL#3 cells collected from the effluent in each outlet (upper and lower microchannels) (Effluent culture) in Pre-VSL#3 vs. Post-VSL#3 in the presence of DSS (2%, wt/vol). (*C*) Assessment of the oxidative stress visualized by the fluorescence probe before (+DSS, Pre-VSL#3) or after the coculture of VSL#3 bacteria (+DSS, Post-VSL#3) in the presence of DSS and PBMC. Quantification of generated ROS using ImageJ ($n = 10$). (*D*) Polarized secretion of the proinflammatory cytokines after 24 h since the PBMC coculture ($n = 4$). Statistical analysis was performed comparing pre- and post-VSL#3 treatment. All experimental groups include PBMC (4×10^6 cells per milliliter). (Scale bar, 50 μm.) NS, not significant. $^*P < 0.05$, $^{**}P < 0.001$, $^{***}P < 0.0001$.

proinflammatory interaction (e.g., recruitment of PBMC on the mucosal area), or microbiome-mediated antiinflammatory therapy (e.g., therapeutic efficacy of probiotic VSL#3) can be visualized and quantified in situ.

DSS has been extensively used in animal colitis models, predominantly in mice (25, 26), to induce mucosal damage and barrier dysfunction followed by microbial translocation (from the lumen to the lamina propria) and immune cell infiltration (from the lamina propria to the lumen). This histological injury and its concomitant immunopathology involve a drastic increase of cytosolic ROS, an elevated level of proinflammatory cytokines in the lamina propria and the plasma, decreased mucus production, a compromised tight junction barrier, and atrophic villus blunting with morphological lesions (25, 26, 43). We confirmed that our gut inflammation-on-a-chip successfully replicated most of these pathophysiological phenotypes and molecular signatures by performing quantitative imaging and biochemical assays. For example, differential interference contrast (DIC) and confocal IF imaging technologies allowed the quantitative assessment of villus height, epithelial cell viability, disposition of the adherens and tight junction proteins, the amount of secretory mucus on the apical brush border, ROS generation, and the recruitment and infiltration of PBMC in situ. Importantly, we discovered that the treatment of DSS to the microengineered villi neither compromises the cell viability nor induces cytotoxicity regardless of the treatment period and the dose. However, DSS treatment specifically induces the barrier dysfunction including the epithelial cell dissociation and detachment, reduction of mucus-producing goblet cells as well as the decreased mucus production, and the loss of tight and adherens junctions, suggesting that the addition of DSS specifically compromises the intestinal barrier function as a negative regulator. We did not observe a complete loss of the basal crypt layer of the epithelium because we performed all of the on-chip experiment in the presence of the microengineered villi, which contain both proliferating and differentiating types (20, 21). Unlike the observation on-chip, DSS treatment caused the complete detachment of Caco-2 cells grown on Transwell and well plates, monitored by changing the Z-position of the focal plane by the confocal microscopy, and thus, the density of remaining bound cells changes as a function of treated DSS concentration.

This observation is technically unique because our on-chip approach can exclude the effect of other interacting factors (e.g., microbiome, immune cells) and focus exclusively on the effect of DSS on the epithelial barrier integrity, which is not possible to realize in any animal models. Indeed, DSS-administered mice showed serious mucosal injuries and inflammation (25, 26), but no studies were able to demonstrate independent uncoupling and control of inflammatory cells. Based on the technical feasibility of our gut inflammation-on-a-chip model, we successfully recapitulated the key pathological outcomes demonstrated in animal models including the recovery of barrier function from pathological colitic symptoms after the cessation of DSS (44, 45), repopulation of mucus-producing goblet cells, and restoration of epithelial structure and barrier function (46). The detached epithelial cells challenged to DSS do not contribute to the reestablishment of 3D villi under physiological flow and mechanical deformations. Hence, we confirmed that the proliferative basal crypt and the spontaneous differentiation of epithelial cells in the gut inflammation-on-a-chip enable the rapid restoration of intestinal barrier function within 1–2 d since the cessation of DSS treatment, which is reminiscent of the wound-healing process in vivo (47).

It has been well characterized that the professional phagocytes in the PBMCs (e.g., monocytes) are the major source of ROS generation (48). Produced ROS including superoxide and hydrogen peroxide are diffusible through an anion channel or aquaporins and induce oxidative stress to the adjacent cells (48, 49). In this study, we found that the cytoplasmic oxidative stress of intestinal epithelium is caused by direct contact with PBMC when the intestinal barrier is dysfunctional due to DSS treatment. Upon direct contact, ROS generated by the PBMCs can diffuse to the barrier-compromised epithelium in an adjacent distance, which further accelerates the accumulation of cytoplasmic ROS in the epithelium. In addition, since the DSS-challenged epithelium undergoes single cell-level disassociation, we hypothesized that the cell-bound adherens junction (e.g., E-cadherin) and tight junction proteins [e.g., coxsackie virus and adenovirus receptor (CAR), occludin, and claudin-1] could be potential ligands to interact with PBMCs upon direct contact. However, a free form of recombinant junctional proteins did not induce ROS generation in response to PBMCs, and only the conditioned medium that contains the dissociated cells released from the DSS-challenged Caco-2 villi showed a significant increase of ROS production. This mechanistic study suggests that the epithelial barrier dysfunction can lead the aberrant interactions with the recruited immune elements and elicit severe oxidative stress in a cell-bound manner.

Nrf2 is a transcription factor that regulates the expression of antioxidative genes and that produces a superoxide dismutase or a glutathione peroxidase in response to tissue oxidative stress followed by the accumulation of cytoplasmic ROS (50, 51). ROS-mediated oxidative stress and inflammation are known to reciprocally affect each other through intracellular signaling pathways such as Nrf2 and NF–κB (29, 52, 53). In our study, we demonstrated the up-regulation of the Nrf2 gene in response to the elevated oxidative stress; however, the oxidative stress alone did not induce the production of inflammatory cytokines by the intestinal inflammatory cells such as the DSS-challenged epithelium or the recruited PBMCs. Interestingly, when the DSS-treated epithelium was simultaneously challenged to either *E. coli* (MOI, 0.25) or LPS at the physiological concentration (31), significant amounts of IL-1β, IL-6, and TNF-α were secreted predominantly to the basolateral side, suggesting that the luminal component derived from the gut microbiome is necessary for the production of inflammatory cytokines. It is notable that the LPS is constitutively detected in the intestinal lumen because the Gram-negative gut bacteria produce bacterial outer membrane vesicles for trafficking bacterial chemicals in other cells (54). Thus, our gut inflammation-on-a-chip clearly demonstrated that this physiological nature might be prone to cause constitutive oxidative stresses and uncontrolled immune responses when the intestinal barrier is dysfunctional.

This report emulates the "homeostatic tolerance" of the intestinal microenvironment by which the intact intestinal barrier and its homeostatic function are necessary and sufficient to suppress the possible inflammatory interactions in healthy individuals. Our current study shows a good agreement with our previous report (24), where the costimulation of LPS and PBMC induced strong immune responses concomitant to the basolateral secretion of proinflammatory cytokines, epithelial injury, villous blunting, and immune cell infiltration. However, it is notable that numerous in vitro studies, including our previous study, have applied a ∼1,000-fold higher concentration of LPS (24, 55) than the amount of LPS typically found in the normal human intestine. This high concentration of LPS indicates that those former studies failed to convey the physiological normal in vivo condition and offered a limited interpretation of the clinical cases such as pathogenic infection with an excessive number of overgrown Gram-negative bacteria (56).

Probiotic therapy is one of the promising clinical options for managing intestinal barrier dysfunction and consequent gut inflammation (57, 58). However, notable challenges have hindered the robust application of probiotic therapy in clinical settings. First, almost all clinical trials have failed to validate the efficacy of probiotic therapy (59–61), whereas both in vitro and in vivo studies have shown promising therapeutic outcomes of probiotic administration (60). Thus, it is important to understand the causality of probiotic efficacy between the model studies versus the clinical outcomes. Second, it has been unclear why probiotic treatment administered to IBD patients who had exacerbated symptoms showed little effects whereas patients in the remission stage showed enhanced probiotic efficacy (33, 60). Finally, it has been challenging to determine the appropriate timing of probiotic administration as a strategic prescription for a probiotic product. All these questions are clinically important but have been poorly answered in previous researches. Our study revealed that the treatment of VSL#3 after barrier dysfunction in the epithelium (i.e., DSS treatment) did not contribute to mitigating inflammatory reactions nor did it help to improve barrier function or mucus production. Rather, it led to unexpected intercellular interactions with PBMC and the aggressive release of IL-1β, IL-6, and TNF-α. On the contrary, VSL#3 treatment before the barrier dysfunction successfully suppressed the secretion of inflammatory cytokines and promoted the repopulation of goblet cells and the mucus production as a "positive regulator" of the barrier function. Since the collective VSL#3 cells or individually isolated genera (i.e., *Bifidobacterium* spp., *Lactobacillus* spp., and *Streptococcus* sp.) can robustly grow in the presence of DSS, we expect that the preinoculated VSL#3 cells will effectively colonize on the mucosal surface and contribute to both the maintenance of barrier homeostasis and the limited production of proinflammatory cytokines. However, the DSS-treated Caco-2 villi led to the compromised villous microarchitecture and atrophic blunting; consequently, the colonization of VSL#3 cells on the DSS-treated villi was greatly challenging. Furthermore, the compromised barrier allows the active transmigration of luminal bacterial cells into the capillary microchannel, so the number of VSL#3 cells in the lumen may decrease. As a consequence, pretreated VSL#3 cells may have a higher chance to prevent the barrier dysfunction caused by DSS. This result implies that probiotic administration may be risky when intestinal barrier function is notably compromised. Indeed, some clinical studies have shown that probiotic treatment to IBD patients with severe symptoms caused serious abdominal infections and probiotic-driven sepsis (32–34, 62). Our study explicitly demonstrated the detrimental effect of intestinal barrier dysfunction on the efficacy of probiotic treatment, which is difficult to replicate in animal models. Taken together, we successfully proved that the maintenance of intact barrier integrity may be the crux of the entire gut inflammatory cascade.

We preliminarily tested the possibility of abnormal or hyperreactive epithelial–immune interactions because the human leukocyte antigen (HLA) incompatibility may cause undesirable immune reactions in response to the different major histocompatibility complex (MHC) of the used human cells. We confirmed that the PBMCs isolated from two independent donor's blood samples did not cause any detectable proinflammatory cytokine productions in Caco-2 epithelial cells. Furthermore, the production profiles of inflammatory cytokines in response to VSL#3 cells (MOI, 0.25) were almost identical in two different batches of PBMCs, confirming that no MHC-dependent abnormal immune response was observed between the sources of PBMC. Thus, we ruled out the possible immune response that may be caused by the MHC difference between Caco-2 cells and PBMCs.

Taken together, these results elucidate that the human gut inflammation-on-a-chip offers an effective approach to selectively manipulate the intestinal barrier integrity, where host–microbiome

cross-talk can be accurately modulated. By utilizing our pathomimetic gut inflammation-on-a-chip, we discovered that barrier dysfunction is one of the most critical triggers that initiates the onset of intestinal inflammation. Maintaining the integrity of the epithelial barrier is necessary and sufficient to suppress mucosal oxidative stress and the subsequent proinflammatory cascades mediated by the aberrant intercellular host–microbiome cross-talk. Our finding suggests that a person with hyperpermeability of the intestinal epithelium, or so-called leaky gut (9), may be more vulnerable to continuous microbial attacks and aggressive immune infiltration, which can lead to a chronic inflammatory stage because the gut can potentially lose its homeostatic tolerance. Our mechanistic study also suggests that targeting the restoration of barrier dysfunction may be a compelling therapeutic approach to effectively control the local inflammation; this approach can be an alternative to neutralizing the tissue-released TNF-α (63) or administering immunomodulatory drugs (64). Ultimately, all of these findings can be replicated with patient-derived primary cells and microbiomes to advance the development of personalized precision medicine.

Materials and Methods

Device Microfabrication. A gut-on-a-chip microfluidic device was made using a soft-lithography method, as described previously (20, 21, 24). Briefly, the upper and lower microchannel layers of a gut-on-a-chip were prepared from cured PDMS [15:1 (wt/wt) prepolymer: curing agent; Sylgard, Dow Corning]. Both upper and lower microchannels have dimensions of $1.0 \times 10 \times 0.2$ mm (width × length × height). A porous PDMS membrane that compartmentalizes the upper and lower microchannels contained an array of holes (10 μm in diameter, 20 μm in thickness, 25 μm spacing) and was produced as described previously (20, 27). Each microchannel was connected to silicone tubing (Tygon 3350, ID 1/32″, OD 3/32″, Beaverton) with a connector (a blunt-end needle, 18G; Kimble Chase) to supply the culture medium. Side vacuum chambers were also linked to the computer-controlled vacuum generator for recreating mechanical deformations.

Microfluidic Cultures. After sterilization by flowing 70% (vol/vol) ethanol into microchannels, the device setup was treated under UV and ozone (UVO; Jelight Company Inc.) for 40 min, followed by coating with collagen type I (0.03 mg/mL) and Matrigel (0.3 mg/mL) for 1 h. A cell culture medium (Dulbecco's modified Eagle medium; Gibco) containing 20% (vol/vol) heat-inactivated FBS (Gibco) and antibiotics (100 U/mL penicillin and 100 μg/mL streptomycin; Gibco) was slowly flowed to ECM-coated channels (50 μL/h) for 12 h. Next, human intestinal epithelial Caco-2BBE cells (Harvard Digestive Disease Center; 1×10^7 cells per milliliter) were seeded to the upper microchannel and incubated at 37 °C in a humidified CO_2 incubator without flow for 1 h. After cell attachment, the culture medium was perfused to the upper microchannel at 50 μL/h (corresponding shear stress, 0.02 dyne/cm^2) for 24–36 h and then switched to both channels once the cells formed a monolayer. Cyclic mechanical motions (10% in cell strain, 0.15 Hz in frequency) were applied by using a Flexcell FX-5000 tension system (Flexcell International Corporation). After a microfluidic culture for 5 d, a Caco-2 monolayer spontaneously formed microengineered villi (20, 21) (TEER > 2 kΩ·cm^2). For host–microbiome coculture, precultured bacterial cells (*SI Appendix*) were introduced to the upper microchannel preconditioned with an antibiotic-free medium for 12 h. Then, the device setup was incubated in the CO_2 incubator without perfusion for 1–2 h for the microbial attachment on the apical surface of the villus epithelium. After microbial attachment, the flow of culture medium was resumed at 50 μL/h under the mechanical strain (10%, 0.15 Hz). PBMC isolated from the deidentified whole blood was used as an immune element.

Modulation of Epithelial Barrier Function. To induce barrier disruption, the culture medium containing DSS (2%, wt/vol; 40 kDa, Sigma-Aldrich) flowed into the upper microchannel at 50 μL/h under mechanical deformations (10%, 0.15 Hz). To stimulate epithelial cells luminally, LPS (from *E. coli* O55: B5; Sigma-Aldrich) was dissolved in the cell culture medium at 10 ng/mL (physiological dose) or 5 μg/mL (excessive dose), or GFP-labeled *E. coli* (seeding density, 1×10^6 cfu/mL; MOI, 0.25) was introduced into the luminal microchannel at 50 μL/h with mechanical motions (10%, 0.15 Hz). PBMC was introduced to the capillary channel as an immune component (seeding density, 4.0×10^6 cells per milliliter). Assessment of epithelial barrier function was performed by measuring the TEER or apparent permeability (P_{app}) (*SI Appendix*).

Morphological Analysis. The morphology of the villus epithelium was observed and recorded using a phase contrast inverted cell culture microscope (DMi1; Leica) and a DIC confocal microscope (DMi8; Leica). Acquired images were processed using LAS X (Leica) or ImageJ.

Assessment of Oxidative Stress. Oxidative stress was evaluated using a CellROX Orange reagent (Thermo Fisher Scientific), a fluorogenic probe (30) that detects epithelial cytoplasmic free radicals. The CellROX reagent that reacts with the cytoplasmic ROS was diluted 250 times in the cell culture medium and infused in both upper and lower microchannels at 30 μL/h, 5% CO_2, 37 °C for 1 h. After the reaction, cells were washed with PBS and then imaged using a confocal laser scanning microscope. The maximum intensity of oxidative stress was estimated by treating H_2O_2 (1 mM) into the cells as a positive control.

Statistical Analysis. A two-tailed unpaired or a two-tailed paired *t* test was performed for statistical analysis. All statistical analysis was carried out using GraphPad Prism 5 (GraphPad Software Inc.). All data and error bars in the article are represented as mean ± SEM. Differences between groups were considered statistically significant when $P < 0.05$ and are indicated with asterisks: $*P < 0.05$, $**P < 0.001$, and $***P < 0.0001$.

ACKNOWLEDGMENTS. We thank Ellington group (University of Texas at Austin) for providing a GFP-labeled *E. coli* strain. This work was supported in part by the Alternatives in Scientific Research of The International Foundation for Ethical Research Graduate Fellowship (UTA15-001318; to W.S.) and the Bio & Medical Technology Development Program of the National Research Foundation (NRF) funded by the Ministry of Science and ICT (2018M3A9H3025030).

1. Graham DY, Opekun AR, Willingham FF, Qureshi WA (2005) Visible small-intestinal mucosal injury in chronic NSAID users. *Clin Gastroenterol Hepatol* 3:55–59.
2. McGuckin MA, Eri R, Simms LA, Florin TH, Radford-Smith G (2009) Intestinal barrier dysfunction in inflammatory bowel diseases. *Inflamm Bowel Dis* 15:100–113.
3. Luster AD, Alon R, von Andrian UH (2005) Immune cell migration in inflammation: Present and future therapeutic targets. *Nat Immunol* 6:1182–1190.
4. Rubin DC, Shaker A, Levin MS (2012) Chronic intestinal inflammation: Inflammatory bowel disease and colitis-associated colon cancer. *Front Immunol* 3:107.
5. Bassotti G, et al. (2014) Gastrointestinal motility disorders in inflammatory bowel diseases. *World J Gastroenterol* 20:37–44.
6. Jurjus AR, Khoury NN, Reimund J-M (2004) Animal models of inflammatory bowel disease. *J Pharmacol Toxicol Methods* 50:81–92.
7. Kiesler P, Fuss IJ, Strober W (2015) Experimental models of inflammatory bowel diseases. *Cell Mol Gastroenterol Hepatol* 1:154–170.
8. Maloy KJ, Powrie F (2011) Intestinal homeostasis and its breakdown in inflammatory bowel disease. *Nature* 474:298–306.
9. Michielan A, D'Incà R (2015) Intestinal permeability in inflammatory bowel disease: Pathogenesis, clinical evaluation, and therapy of leaky gut. *Mediators Inflamm* 2015: 628157.
10. Packey CD, Sartor RB (2009) Commensal bacteria, traditional and opportunistic pathogens, dysbiosis and bacterial killing in inflammatory bowel diseases. *Curr Opin Infect Dis* 22:292–301.
11. Atreya I, Atreya R, Neurath MF (2008) NF-kappaB in inflammatory bowel disease. *J Intern Med* 263:591–596.
12. Lasry A, Zinger A, Ben-Neriah Y (2016) Inflammatory networks underlying colorectal cancer. *Nat Immunol* 17:230–240.
13. Herías MV, Koninkx JF, Vos JG, Huis in't Veld JH, van Dijk JE (2005) Probiotic effects of Lactobacillus casei on DSS-induced ulcerative colitis in mice. *Int J Food Microbiol* 103: 143–155.
14. Sainathan SK, et al. (2008) Granulocyte macrophage colony-stimulating factor ameliorates DSS-induced experimental colitis. *Inflamm Bowel Dis* 14:88–99.
15. Morris GP, et al. (1989) Hapten-induced model of chronic inflammation and ulceration in the rat colon. *Gastroenterology* 96:795–803.
16. Kühn R, Löhler J, Rennick D, Rajewsky K, Müller W (1993) Interleukin-10-deficient mice develop chronic enterocolitis. *Cell* 75:263–274.
17. Onizawa M, et al. (2009) Signaling pathway via TNF-alpha/NF-kappaB in intestinal epithelial cells may be directly involved in colitis-associated carcinogenesis. *Am J Physiol Gastrointest Liver Physiol* 296:G850–G859.
18. Morrissey PJ, Charrier K, Braddy S, Liggitt D, Watson JD (1993) CD4+ T cells that express high levels of CD45RB induce wasting disease when transferred into congenic severe combined immunodeficient mice. Disease development is prevented by cotransfer of purified CD4+ T cells. *J Exp Med* 178:237–244.
19. Telang N, Katdare M (2007) Cell culture model for colon cancer prevention and therapy: An alternative approach to animal experimentation. *ALTEX* 24:16–21.
20. Kim HJ, Huh D, Hamilton G, Ingber DE (2012) Human gut-on-a-chip inhabited by microbial flora that experiences intestinal peristalsis-like motions and flow. *Lab Chip* 12:2165–2174.

21. Kim HJ, Ingber DE (2013) Gut-on-a-chip microenvironment induces human intestinal cells to undergo villus differentiation. *Integr Biol* 5:1130–1140.
22. Park G-S, et al. (2017) Emulating host-microbiome ecosystem of human gastrointestinal tract in vitro. *Stem Cell Rev* 13:321–334.
23. Bein A, et al. (2018) Microfluidic organ-on-a-chip models of human intestine. *Cell Mol Gastroenterol Hepatol* 5:659–668.
24. Kim HJ, Li H, Collins JJ, Ingber DE (2016) Contributions of microbiome and mechanical deformation to intestinal bacterial overgrowth and inflammation in a human gut-on-a-chip. *Proc Natl Acad Sci USA* 113:E7–E15.
25. Solomon L, et al. (2010) The dextran sulphate sodium (DSS) model of colitis: An overview. *Comp Clin Pathol* 19:235–239.
26. Chassaing B, Aitken JD, Malleshappa M, Vijay-Kumar M (2014) Dextran sulfate sodium (DSS)-induced colitis in mice. *Curr Protoc Immunol* 104:15.25.1–15.25.14.
27. Kim HJ, Lee J, Choi JH, Bahinski A, Ingber DE (2016) Co-culture of living microbiome with microengineered human intestinal villi in a gut-on-a-chip microfluidic device. *J Vis Exp* e54344.
28. Kuo JC, et al. (2016) Detection of colorectal dysplasia using fluorescently labelled lectins. *Sci Rep* 6:24231.
29. Piechota-Polanczyk A, Fichna J (2014) Review article: The role of oxidative stress in pathogenesis and treatment of inflammatory bowel diseases. *Naunyn Schmiedebergs Arch Pharmacol* 387:605–620.
30. O'Connor J-E, et al. (2017) Cytomics of oxidative stress: Probes and problems. *Single Cell Analysis* (Springer, Singapore), pp 83–118.
31. Guo S, et al. (2015) Lipopolysaccharide regulation of intestinal tight junction permeability is mediated by TLR4 signal transduction pathway activation of FAK and MyD88. *J Immunol* 195:4999–5010.
32. Farina C, Arosio M, Mangia M, Moioli F (2001) Lactobacillus casei subsp. rhamnosus sepsis in a patient with ulcerative colitis. *J Clin Gastroenterol* 33:251–252.
33. Kunz AN, Noel JM, Fairchok MP (2004) Two cases of Lactobacillus bacteremia during probiotic treatment of short gut syndrome. *J Pediatr Gastroenterol Nutr* 38:457–458.
34. Liong M-T (2008) Safety of probiotics: Translocation and infection. *Nutr Rev* 66: 192–202.
35. Shim K-Y, et al. (2017) Microfluidic gut-on-a-chip with three-dimensional villi structure. *Biomed Microdevices* 19:37.
36. Wang Y, et al. (2018) Bioengineered systems and designer matrices that recapitulate the intestinal stem cell niche. *Cell Mol Gastroenterol Hepatol* 5:440–453.e1.
37. Shah P, et al. (2016) A microfluidics-based in vitro model of the gastrointestinal human-microbe interface. *Nat Commun* 7:11535.
38. Jalili-Firoozinezhad S, et al. (2018) Modeling radiation injury-induced cell death and countermeasure drug responses in a human gut-on-a-chip. *Cell Death Dis* 9:223.
39. Mittal M, Siddiqui MR, Tran K, Reddy SP, Malik AB (2014) Reactive oxygen species in inflammation and tissue injury. *Antioxid Redox Signal* 20:1126–1167.
40. Kontoyiannis D, Pasparakis M, Pizarro TT, Cominelli F, Kollias G (1999) Impaired on/off regulation of TNF biosynthesis in mice lacking TNF AU-rich elements: Implications for joint and gut-associated immunopathologies. *Immunity* 10:387–398.
41. Sundberg JP, Elson CO, Bedigian H, Birkenmeier EH (1994) Spontaneous, heritable colitis in a new substrain of C3H/HeJ mice. *Gastroenterology* 107:1726–1735.
42. Rivera-Nieves J, et al. (2003) Emergence of perianal fistulizing disease in the SAMP1/YitFc mouse, a spontaneous model of chronic ileitis. *Gastroenterology* 124:972–982.
43. Perše M, Cerar A (2012) Dextran sodium sulphate colitis mouse model: Traps and tricks. *J Biomed Biotechnol* 2012:718617.
44. Mähler M, et al. (1998) Differential susceptibility of inbred mouse strains to dextran sulfate sodium-induced colitis. *Am J Physiol* 274:G544–G551.
45. Yan Y, et al. (2009) Temporal and spatial analysis of clinical and molecular parameters in dextran sodium sulfate induced colitis. *PLoS One* 4:e6073.
46. Melgar S, Karlsson A, Michaëlsson E (2005) Acute colitis induced by dextran sulfate sodium progresses to chronicity in C57BL/6 but not in BALB/c mice: Correlation between symptoms and inflammation. *Am J Physiol Gastrointest Liver Physiol* 288: G1328–G1338.
47. Iizuka M, Konno S (2011) Wound healing of intestinal epithelial cells. *World J Gastroenterol* 17:2161–2171.
48. Aruoma OI (1998) Free radicals, oxidative stress, and antioxidants in human health and disease. *J Am Oil Chem Soc* 75:199–212.
49. Nishiyama Y, Kataoka T, Yamato K, Taguchi T, Yamaoka K (2012) Suppression of dextran sulfate sodium-induced colitis in mice by radon inhalation. *Mediators Inflamm* 2012:239617.
50. Jones RM, Mercante JW, Neish AS (2012) Reactive oxygen production induced by the gut microbiota: Pharmacotherapeutic implications. *Curr Med Chem* 19:1519–1529.
51. Ma Q (2013) Role of nrf2 in oxidative stress and toxicity. *Annu Rev Pharmacol Toxicol* 53:401–426.
52. Biswas SK (2016) Does the interdependence between oxidative stress and inflammation explain the antioxidant paradox? *Oxid Med Cell Longev* 2016:5698931.
53. Buelna-Chontal M, Zazueta C (2013) Redox activation of Nrf2 & NF-κB: A double end sword? *Cell Signal* 25:2548–2557.
54. Raetz CR, Whitfield C (2002) Lipopolysaccharide endotoxins. *Annu Rev Biochem* 71: 635–700.
55. Yu LC, Flynn AN, Turner JR, Buret AG (2005) SGLT-1-mediated glucose uptake protects intestinal epithelial cells against LPS-induced apoptosis and barrier defects: A novel cellular rescue mechanism? *FASEB J* 19:1822–1835.
56. Im E, Riegler FM, Pothoulakis C, Rhee SH (2012) Elevated lipopolysaccharide in the colon evokes intestinal inflammation, aggravated in immune modulator-impaired mice. *Am J Physiol Gastrointest Liver Physiol* 303:G490–G497.
57. Dai C, Zhao D-H, Jiang M (2012) VSL#3 probiotics regulate the intestinal epithelial barrier in vivo and in vitro via the p38 and ERK signaling pathways. *Int J Mol Med* 29: 202–208.
58. Madsen K, et al. (2001) Probiotic bacteria enhance murine and human intestinal epithelial barrier function. *Gastroenterology* 121:580–591.
59. Isaacs K, Herfarth H (2008) Role of probiotic therapy in IBD. *Inflamm Bowel Dis* 14: 1597–1605.
60. Claes IJ, De Keersmaecker SC, Vanderleyden J, Lebeer S (2011) Lessons from probiotic-host interaction studies in murine models of experimental colitis. *Mol Nutr Food Res* 55:1441–1453.
61. Prantera C, Scribano ML, Falasco G, Andreoli A, Luzi C (2002) Ineffectiveness of probiotics in preventing recurrence after curative resection for Crohn's disease: A randomised controlled trial with Lactobacillus GG. *Gut* 51:405–409.
62. Boyle RJ, Robins-Browne RM, Tang ML (2006) Probiotic use in clinical practice: What are the risks? *Am J Clin Nutr* 83:1256–1264, quiz 1446–1447.
63. Ordás I, Mould DR, Feagan BG, Sandborn WJ (2012) Anti-TNF monoclonal antibodies in inflammatory bowel disease: Pharmacokinetics-based dosing paradigms. *Clin Pharmacol Ther* 91:635–646.
64. Gisbert JP, Gomollón F, Maté J, Pajares JM (2002) Role of 5-aminosalicylic acid (5-ASA) in treatment of inflammatory bowel disease: A systematic review. *Dig Dis Sci* 47: 471–488.